

Moment-based analysis of biochemical feedback circuits in a population of chemically interacting cells

David T. Gonzales^{1,2}, T-Y Dora Tang¹, and Christoph Zechner^{1,2,3}

¹Max Planck Institute of Molecular Cell Biology and Genetics, 01307 Dresden, Germany

²Center for Systems Biology Dresden, 01307 Dresden, Germany

³Correspondence to: zechner@mpi-cbg.de

Cells utilize chemical communication to exchange information and coordinate their behavior in noisy environments. Depending on the scenario, communication can reduce variability and shape a collective response, or amplify variability to generate distinct phenotypic subpopulations. Here we use a moment-based approach to study how cell-cell communication affects noise in biochemical networks that arises from both intrinsic and extrinsic sources. Based on a recently proposed model reduction technique, we derive a system of differential equations that captures lower-order moments of a population of cells, which communicate by secreting and sensing a diffusing molecule. Importantly, the number of equations that we obtain in this way is independent of the number of considered cells such that the method scales to arbitrary population sizes. Based on this approach, we analyze how cell-cell communication affects noise in several biochemical circuits.

1 Introduction

In recent years, significant progress has been made in developing computational models and algorithms to study stochastic biochemical networks inside living cells. Most commonly, these models are based on the chemical master equation (CME), whose solution provides a time-dependent probability distribution over molecular concentrations [1]. CME-based models can faithfully account for the discrete and random nature of biochemical reactions (intrinsic noise) as well as additional heterogeneity stemming from differences in each cell's microenvironment (extrinsic variability) [2, 3]. The computational analysis of the CME is associated with certain difficulties but by now, there exists a repertoire of efficient numerical techniques including stochastic Monte Carlo algorithms [1], moment-based methods [4, 5] and combinations thereof [6, 7, 8].

However, the vast majority of existing approaches to study noise in cell populations rely on the assumption that individual cells act independently of each other. More concretely, each cell's dynamics is considered to be an independent and identically distributed realization of the same stochastic process. Evidently, this assumption is violated in multicellular systems, where cells communicate with one another to coordinate their behavior [9, 10]. Typical examples include quorum-sensing systems in bac-

terial colonies [11], or paracrine communication in higher organisms [12]. Understanding the interplay between cell-cell communication and the stochastic behavior of individual cells is an important challenge and demands for suitable mathematical approaches. However, extending existing techniques to account for cell-cell communication leads to computational difficulties, because the dimensionality of the resulting models increases with the number of cells in a population.

Recently, first attempts have been made to develop more tractable models of stochastic multicellular systems. In [9], for instance, the authors use a moment-based method to study how neighbour-neighbour-coupling affects concentration fluctuations in a tissue. A related approach has been proposed in [13] to study community effects in cells that interact with each other by secreting and sensing certain signalling molecules. In particular, the authors show how the dimensionality of multicellular models can be dramatically reduced by exploiting certain symmetries in the governing equations. However, both approaches account exclusively for intrinsic noise, whereas extrinsic sources have not been considered. In another recent work [14], the authors study how chemical communication via a quorum sensing molecule affects intrinsic and extrinsic noise in cell communities. To obtain tractable simulations, the authors used a tailored approach that combines stochastic simulations with a quasi-steady state approximation to eliminate fast variables from the model.

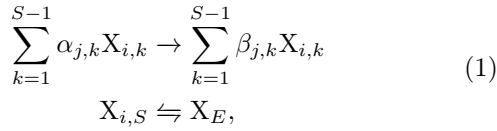
In this article, we present a general moment-based approach to study biochemical circuits in populations of chemically interacting cells. In particular, we focus on a secrete-and-sense model [10], where individuals can secrete signalling molecules to the extracellular environment, which in turn can be sensed by other cells in the population. Importantly, our model accounts for both intrinsic and extrinsic variability. Similar to [13], we exploit certain symmetries of the model to derive a system of moment-equations that is independent of the population size and thus computationally very efficient. This approach allowed us to study the interplay between noise and cell-to-cell communication in several nonlinear biochemical circuits.

The rest of the paper is structured as follows. A general model of biochemical networks in chemically interacting cell populations is presented in Section 2. In Section 3, we provide a stochastic description of this model based on the CME and derive a general equation for its moment

dynamics. In Section 4, we show how the number of moment equations can be reduced by exploiting symmetries of the model. Finally, we apply our approach to analyze several biochemical circuits in Section 5.

2 Reaction networks in a population of chemically interacting cells

We consider a population of N genetically identical cells that communicate with each other through a diffusing signalling molecule (Fig. 1). Each individual cell i is associated with an identical set of S chemical species $X_{i,1}, \dots, X_{i,S}$ that interact with one another via M biochemical reaction channels. Without loss of generality, we consider the first $S - 1$ species to be confined to the intracellular environment of cell i . The S th species corresponds to the signalling molecule, which can shuttle between the intra- and extracellular environment through transport reactions. For simplicity, we consider the external environment to be well-mixed, such that the import of signalling molecules into any cell i does not depend on the spatial configuration of the system. In total, the system can be described by a reaction network



for $i = 1, \dots, N$ and $j = 1, \dots, M - 1$. In (1), $\alpha_{j,k}$ and $\beta_{j,k}$ correspond to the reactant and product coefficients of the respective reaction. The species X_E denotes the signalling molecule in the external environment.

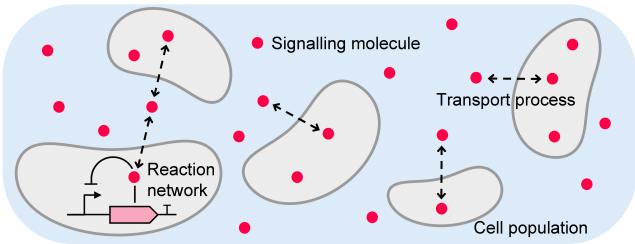


Figure 1: Secrete-and-sense model of cell populations. Each cell's dynamics is described by the same reaction network, whereas one of the reactants serves as a signalling molecule (red). The latter can diffuse to the homogeneous extracellular environment from where it can be sensed again by any of the cells.

In total, the network comprises $NS + 1$ chemical species and NM chemical reactions. We define by $X_i(t) = (X_{i,1}(t), \dots, X_{i,S}(t))$ the state of cell i , which collects the copy numbers of all species associated with this cell at time t . The state of the overall system is then given by $X(t) = (X_1(t), \dots, X_N(t), X_E(t))$, with $X_E(t)$ as the number of signalling molecules in the external environment. Moreover, we denote by $\nu_{i,k} \in \mathbb{Z}^{NS+1}$ the stoichiometric change vector associated with the k th reaction channel of cell i consistent with reaction network (1).

3 Moment dynamics of heterogeneous cell communities

If both the intra- and extracellular environments are well-mixed, we can describe the state $X(t)$ as a continuous-time Markov chain (CTMC), whose state probability distribution $P(x, t) = P(X(t) = x)$ admits a master equation of the form

$$\frac{dP(x, t)}{dt} = \sum_{i=1}^N \sum_{j=1}^M [a_j(x - \nu_{i,j}, c_{i,j}) P(x - \nu_{i,j}, t) - a_j(x, c_{i,j}) P(x, t)]. \quad (2)$$

In (2), the function a_j is the reaction propensity associated with reaction j . Throughout this article, we consider the propensities to obey the law of mass action such that $a_j(x, c_{i,j}) = c_{i,j} g_j(x)$ with $c_{i,j}$ as a stochastic rate constant and g_j a polynomial determined by the stoichiometry of this reaction. Note that while g_j is identical for all cells, we allow the individual rate constants $c_{i,j}$ to vary across the population. This provides a means to account for extrinsic sources of cell-to-cell variability that may contribute to the overall population heterogeneity [5]. More precisely, we consider the reaction rate constants for each cell to be independent random vectors $C_i = (C_{i,1}, \dots, C_{i,M})$ drawn from a common probability distribution $C_i \sim p_c(\cdot)$ for $i = 1, \dots, N$. Note that deterministic (non-varying) reaction rates can be accounted for by letting p_c be a Dirac measure with respect to this parameter. With $C = (C_1, \dots, C_N)$, we can then formulate a master equation for the conditional distribution $P(x, t | c) = P(X(t) = x | C = c)$, i.e.,

$$\frac{dP(x, t | c)}{dt} = \sum_{i=1}^N \sum_{j=1}^M [a_{i,j}(x - \nu_{i,j}, c_{i,j}) P(x - \nu_{i,j}, t | c) - a_{i,j}(x, c_{i,j}) P(x, t | c)]. \quad (3)$$

3.1 Moment dynamics

For the sake of tractability, we resort to a moment-based approach, which provides a lower-dimensional description of the population and its heterogeneity. More precisely, we seek for the population moments

$$\begin{aligned} \langle \phi(X) \rangle &= \langle \langle \phi(X) | C \rangle \rangle \\ &= \left\langle \sum_{x \in \mathcal{X}} \phi(x) P(x, t | C) \right\rangle, \end{aligned} \quad (4)$$

with $\phi : x \rightarrow \mathbb{Z}$ as a monomial in x and \mathcal{X} as the domain of $X(t)$. Note that the outer expectation in (4) is taken with respect to the distribution p_c . In order to derive a differential equation for the time evolution of $\langle \phi(X(t)) \rangle$, we calculate the derivative of (4) and insert the r.h.s. of (3)

$$\frac{d}{dt} \langle \phi(X) \rangle = \left\langle \sum_{x \in \mathcal{X}} \phi(x) \sum_{i=1}^N \sum_{j=1}^M [a_j(x - \nu_{i,j}, C_{i,j}) P(x - \nu_{i,j}, t | C) - a_j(x, C_{i,j}) P(x, t | C)] \right\rangle. \quad (5)$$

Table 1: Normal & lognormal closure functions of order three.

MA	$\langle X_1 X_2 X_3 \rangle$
Normal	$\langle X_1 \rangle \langle X_2 X_3 \rangle + \langle X_2 \rangle \langle X_1 X_3 \rangle$ $+ \langle X_3 \rangle \langle X_1 X_2 \rangle - 2 \langle X_1 \rangle \langle X_2 \rangle \langle X_3 \rangle$
Lognormal	$\frac{\langle X_1 X_2 \rangle \langle X_2 X_3 \rangle \langle X_1 X_3 \rangle}{\langle X_1 \rangle \langle X_2 \rangle \langle X_3 \rangle}$

Using a change of variable, it is straightforward to show that (5) simplifies to

$$\frac{d}{dt} \langle \phi(X) \rangle = \left\langle \sum_{i=1}^N \sum_{j=1}^M \left\langle \phi(X + \nu_{i,j}) a_j(X, C_{i,j}) \mid C \right\rangle - \left\langle \phi(X) a_j(X, C_{i,j}) \mid C \right\rangle \right\rangle, \quad (6)$$

where the inner brackets denote expectations conditionally on the random parameters C . Now, using double expectations, we obtain

$$\frac{d}{dt} \langle \phi(X) \rangle = \sum_{i=1}^N \sum_{j=1}^M \left\langle \phi(X + \nu_{i,j}) a_j(X, C_{i,j}) \right\rangle - \left\langle \phi(X) a_j(X, C_{i,j}) \right\rangle. \quad (7)$$

Eq. (7) describes the time evolution of moments and cross moments for a heterogeneous population of secrete-and-sense cells. It can thus be seen as a multicellular extension of the moment equations derived in [5]. Indeed, if we set the transport rates to zero, all cells in the population become independent of each other such that the two approaches coincide.

Note that depending on the stoichiometry of the system, the system of equations (7) may not be closed. For instance, this is the case in the presence of higher-order reactions, or even first-order reactions if their rate constants are randomly distributed across the population. Moment-closure techniques provide a popular means to address this problem by imposing certain assumptions on the underlying state probability distribution [4, 5, 15]. More precisely, this allows us to replace the higher order moments that appear on the r.h.s. of (7) by functions of the lower order moments. These functions are referred to as *closure functions* and their particular form depends on the distributional assumption we make. Popular choices include the normal [15] and lognormal [4] closure functions and we will adopt those in the present study. Throughout this article, we consider moments of first and second order and correspondingly, replace all third-order moments that appear on the r.h.s. of (7) using the respective closure functions provided in Table 1.

4 Symmetry-based model reduction

While eq. (7) provides a more tractable description of the cell community than (2), its dimensionality still scales quadratically with the number of considered cells N . In case we consider all first and second order moments, the

number of equations is given by

$$K_{eq} = 2(NS + 1) + \binom{NS + NM + 1}{2}. \quad (8)$$

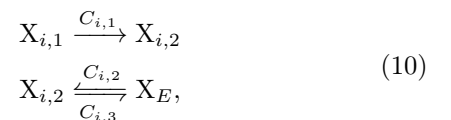
For instance, if we consider a heterogeneous community of $N = 5$ cells, with $S = 3$ chemical species and $M = 2$ reactions, we would need to solve $K_{eq} = 357$ differential equations. Clearly, this limits the above approach to relatively small population sizes. However, the number of equations can be dramatically reduced by taking into account the symmetries of the considered model as has been proposed in [13]. More precisely, if we consider all initial cell states $X_i(0)$ to be identically distributed, the moment dynamics of each cell will be equivalent and indistinguishable for all times $t > 0$ such that $\langle X_{i,k} \rangle = \langle X_{j,k} \rangle$, $\langle X_{i,k} X_{j,l} \rangle = \langle X_{m,k} X_{n,l} \rangle$ and $\langle X_{i,k} X_E \rangle = \langle X_{j,k} X_E \rangle$ for any i, j, m, n, k and l . Consequently, the cell community can be effectively described by considering the moments and cross-moments of any two reference cells $X_i(t)$ and $X_j(t)$ as well as the amount of signalling molecule in the external environment $X_E(t)$. The required number of equations then amounts to

$$\hat{K}_{eq} = 4S + 2 + \binom{2S + 2M + 1}{2}, \quad (9)$$

and is thus independent of the population size. We will next illustrate the reduction of moment equations using a simple example.

4.1 Illustrative example

Consider the toy model



with $i = 1, \dots, N$. We assume that the conversion rate $C_{i,1}$ and transport rates $C_{i,2}$ and $C_{i,3}$ are randomly distributed across the population.

To demonstrate how the original system can be reduced based on symmetries, we distinguish between two different cases. The first case concerns equations that are the same in the original and reduced model. These involve the dynamics of species that do not directly depend on the signalling molecule in the external environment such as $\langle X_{i,1} \rangle$, $\langle X_{i,2} \rangle$, or $\langle X_{i,1} X_{i,2} \rangle$. For example, in both the original and reduced models, the expectation of species $X_{i,2}$ satisfies

$$\frac{d\langle X_{i,2} \rangle}{dt} = \langle C_{i,1} X_{i,1} \rangle + \langle C_{i,2} X_E \rangle - \langle C_{i,3} X_{i,2} \rangle. \quad (11)$$

Moments and cross-moments involving the external signalling molecule are affected by *all* cells in the population due to the transport reactions. In the case of $\langle X_{i,2} X_E \rangle$, the original equation is:

$$\begin{aligned}
\frac{d\langle X_{i,2}X_E \rangle}{dt} &= \langle C_{i,1}X_{1,1}X_E \rangle \\
&- \sum_{j=1}^N [\langle C_{j,2}X_E^2 \rangle - \langle C_{j,2}X_{j,2} \rangle - \langle C_{j,2} \rangle] \\
&+ \sum_{j=1}^N [\langle C_{j,3}X_{j,2}^2 \rangle - \langle C_{j,3}X_E \rangle - \langle C_{j,3} \rangle].
\end{aligned} \tag{12}$$

For the reduced model, we rewrite (12) as

$$\begin{aligned}
\frac{d\langle X_{i,2}X_E \rangle}{dt} &= \langle C_{i,1}X_{1,1}X_E \rangle \\
&- [\langle C_{i,2}X_E^2 \rangle - \langle C_{i,2}X_{i,2} \rangle - \langle C_{i,2} \rangle] \\
&+ [\langle C_{i,3}X_{i,2}^2 \rangle - \langle C_{i,3}X_E \rangle - \langle C_{i,3} \rangle] \\
&- \sum_{j \neq i} [\langle C_{j,2}X_E^2 \rangle - \langle C_{j,2}X_{j,2} \rangle - \langle C_{j,2} \rangle] \\
&+ \sum_{j \neq i} [\langle C_{j,3}X_{j,2}^2 \rangle - \langle C_{j,3}X_E \rangle - \langle C_{j,3} \rangle].
\end{aligned} \tag{13}$$

Now, since all terms in the two sums are identical due to the symmetry of the population, they can be replaced by the contribution of any cell j multiplied by $N - 1$, i.e.,

$$\begin{aligned}
\frac{d\langle X_{i,2}X_E \rangle}{dt} &= \langle C_{i,1}X_{1,1}X_E \rangle \\
&- [\langle C_{i,2}X_E^2 \rangle - \langle C_{i,2}X_{i,2} \rangle - \langle C_{i,2} \rangle] \\
&+ [\langle C_{i,3}X_{i,2}^2 \rangle - \langle C_{i,3}X_E \rangle - \langle C_{i,3} \rangle] \\
&- (N - 1) [\langle C_{j,2}X_E^2 \rangle - \langle C_{j,2}X_{j,2} \rangle - \langle C_{j,2} \rangle] \\
&+ (N - 1) [\langle C_{j,3}X_{j,2}^2 \rangle - \langle C_{j,3}X_E \rangle - \langle C_{j,3} \rangle].
\end{aligned} \tag{14}$$

Therefore, if we perform analogous manipulations for the remaining moments and cross-moments, we obtain a reduced moment-based description that involves only the species of two reference cells i and j , as well as the signalling molecule in the external environment X_E .

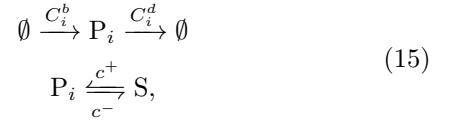
5 Case studies

In this section, we use the described moment-based approach to study how cell-cell communication affects noise in different biochemical circuits. We show that this approach can accurately capture lower-order moments of heterogeneous communicating cell populations containing stochastic chemical reactions and compare them to moments estimated from SSA simulations. In addition, we study how the signalling transport rate, the population size, and extrinsic variability affect the heterogeneity of the population.

Python scripts to implement the model and run stochastic simulations used the packages Sympy (www.sympy.org) [16] and Tellerium (www.tellerium.analogmachine.org) [17]. For the sake of a compact notation, molecular species are assigned different letters and reaction rate parameters are assigned letters with superscripts.

5.1 Birth-death process

As a first example, we study a birth-death process in a heterogeneous population of interacting cells, i.e.,



for $i = 1, \dots, N$. Here, the birth- and death reaction rate constants are considered to be randomly distributed across the population as indicated by capital letters C_i^b and C_i^d . For this reaction network, a symmetry-reduced model of up to the second order can be described using $\hat{K}_{eq} = 27$ differential equations regardless of the population size.

The goal of this case study is to observe how cell-to-cell communication affects the variability in the abundance of P_i . To quantify variability, we use two metrics: the first one is the coefficient of variation (CV) defined as

$$\text{CV}[P_i] = \sqrt{\frac{\langle P_i^2 \rangle - \langle P_i \rangle^2}{\langle P_i \rangle^2}}, \tag{16}$$

for any $i = 1, \dots, N$. The CV captures the expected variation in protein abundance inside single cells across *different* populations. Due to the symmetry, we have $\text{CV}[P_i] = \text{CV}[P_j]$ for any $i \neq j$. Furthermore, we define the pair variation (PV)

$$\text{PV}[P_i, P_j] = \sqrt{\frac{\langle (P_i - P_j)^2 \rangle}{\langle P_i \rangle \langle P_j \rangle}}, \tag{17}$$

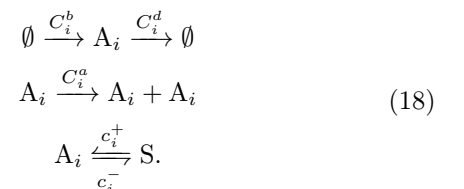
which captures the expected variation between two different cells i and j within the *same* population. Note that in the absence of cell-cell communication, (16) and (17) are identical up to a scaling factor of $\sqrt{2}$. For a coupled population, however, this is not the case, due to correlations between individual cells in the population.

Figs. 2A and B show stochastic realizations of the system for $N = 50$ and compares them to the approximate moments obtained from the symmetry-reduced model. In Figs. 2C-F we show the dependency of the CV and PV as a function of the transport rates as well as the population size. We found that the CV decreases with increasing transport rates and population size. While we observe a similar inverse relation between the PV and the transport rates, the former is more or less independent of the population size.

We also show how extrinsic noise changes the steady-state variability by increasing the CV of the birth rate parameter C^b , while keeping all other parameters constant. Both the CV and PV increase with increasing extrinsic noise, whereas large coupling rates can attenuate this effect (Fig. 3).

5.2 Autocatalytic circuit

Next, we focus on an autocatalytic system defined by



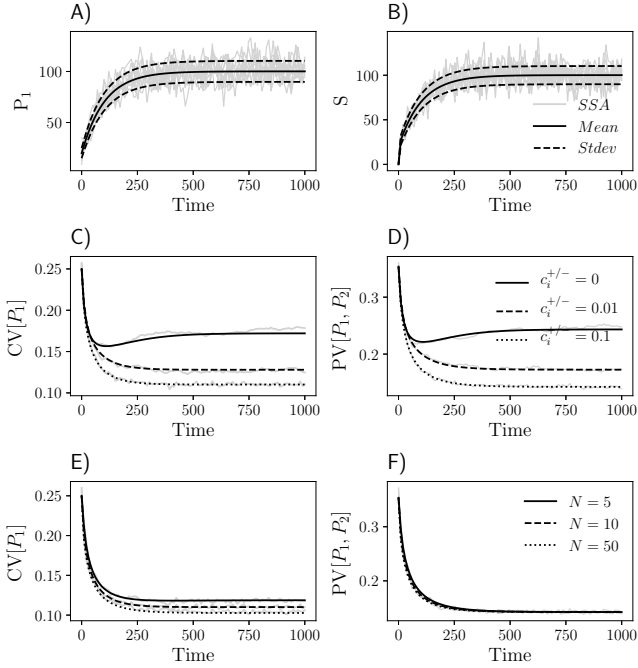


Figure 2: Birth-death moment dynamics generated by the symmetry-reduced model (Gaussian MA) with 10 representative SSA simulations for species P_1 (A) and S (B) with a population size of $N = 50$ and $c^{+/-} = 0.1$. $CV[P_1]$ and $PV[P_1, P_2]$ decrease as transport rate increases $c^{+/-} = [0, 0.01, 0.1]$ for a fixed population size $N = 10$ (C and D). Increasing the population size $N = [5, 10, 50]$ for a fixed $c^{+/-} = 0.1$ decreases the $CV[P_1]$, but not $PV[P_1, P_2]$ (E and F). Other parameters and initial conditions are set as $\langle C_i^b \rangle = 1$, $\text{Var}[C_i^b] = 0.01$, $\langle C_i^d \rangle = 0.01$, $\text{Var}[C_i^d] = 1e - 6$, $\langle P_i(0) \rangle = 20$, $\text{Var}[P_i(0)] = 25$, $\langle S(0) \rangle = 0$, and $\text{Var}[S(0)] = 0$. Grey colored traces in C-F are calculated from 2000 SSA realizations with parameter settings matching their respective moment dynamics in black.

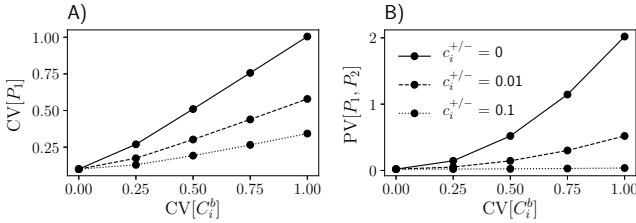


Figure 3: Steady-state $CV[P_1]$ (A) and $PV[P_1, P_2]$ (B) for varying coupling rates ($c^{+/-}$) and population heterogeneity ($CV[C_i^b]$). Other parameters and initial conditions are set as $\langle C_i^b \rangle = 1$, $c^d = 0.01$, $\langle P_i(0) \rangle = 20$, $\text{Var}[P_i(0)] = 25$, $\langle S(0) \rangle = 0$, and $\text{Var}[S(0)] = 0$. The population size is $N = 10$ and steady-state moments were determined from a symmetry-reduced model with Gaussian closure at $t = 1000$.

Here we consider C_i^b , C_i^d and C_i^a to be randomly distributed across the population. To obtain a closed set of moments, we applied the lognormal closure. We first tested the accuracy of this closure by comparing it to Monte Carlo estimates of the moments calculated over 5000 SSA realizations (Fig. 4). We generally found a good agreement between the moment-approximation and the SSA simulation, whereas we see a certain degree of mismatch for very low transport rates (Fig. 4C and D). Similar to the previous case study, we observe that the CV of species A_i is inversely related to the transport rates and

the population size. Again, the PV is largely independent of the population size but can be decreased by enhanced transport.

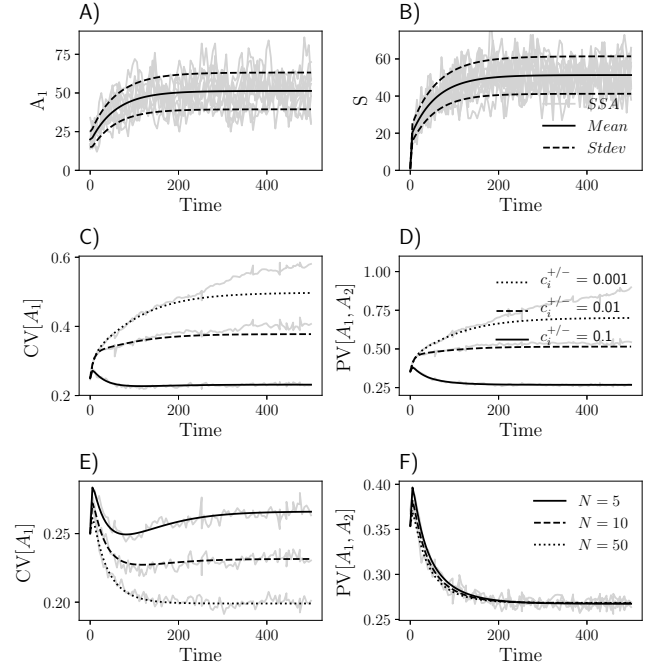
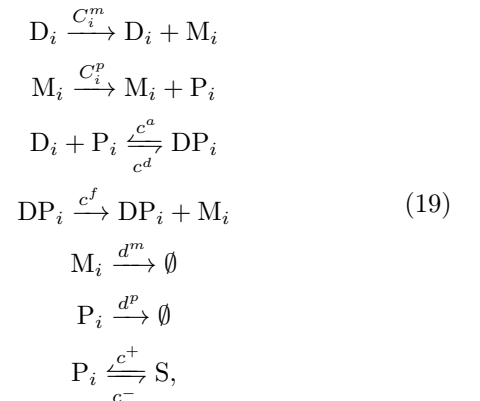


Figure 4: Autocatalytic moment dynamics generated by the symmetry-reduced model (Lognormal MA) with 10 representative SSA simulations for species A_1 (A) and S (B) for a population size of $N = 50$ and $c^{+/-} = 0.1$. $CV[A_1]$ and $PV[A_1, A_2]$ decrease as transport rate increases from $c^{+/-} = [0, 0.01, 0.1]$ for a fixed population size $N = 10$ (C and D). Increasing the population size from $N = [5, 10, 50]$ for a fixed $c^{+/-} = 0.1$ decreases the $CV[A_1]$ (E), while $PV[A_1, A_2]$ increases a minimal amount (F). Other parameters and initial conditions are set to $\langle C_i^b \rangle = 1$, $\text{Var}[C_i^b] = 0.01$, $\langle C_i^a \rangle = 0.08$, $\text{Var}[C_i^a] = 6.4e - 5$, $\langle C_i^d \rangle = 0.1$, $\text{Var}[C_i^d] = 1e - 4$, $\langle A_i(0) \rangle = 20$, $\text{Var}[A_i(0)] = 25$, $\langle S(0) \rangle = 0$, and $\text{Var}[S(0)] = 0$. Grey colored traces in (C-F) are calculated from 5000 SSA realizations.

5.3 Genetic feedback circuit

In the last example, we tested the moment-based method using a larger system. In particular, we focus on a genetic feedback circuit given by



for $i = 1, \dots, N$. Here, we consider the reaction rate constants associated with transcription C_i^m and translation C_i^p to be randomly distributed across the population. Transcriptional feedback of the gene circuit is mediated by the protein product (P), which binds DNA (D) to form

a complex DP. In the bound state, the gene can be transcribed with rate constant c^f . Depending on the ratio of the bound and unbound transcription rate, the feedback mechanism can either enhance ($c^f > \langle C_i^m \rangle$) or inhibit ($c^f < \langle C_i^m \rangle$) gene expression. We consider a population of $N = 10$ cells, in which case the number of equations would be $K_{eq} = 1912$ for the original model. For the reduced model, we obtain $\hat{K}_{eq} = 96$ equations, then applied the lognormal closure function. Fig 5 shows the time evolution of the moments of mRNA obtained from the symmetry-reduced model and compares it to Monte Carlo estimates obtained from SSA. We found that for both positive and negative feedback, the approximate moment dynamics accurately capture the dynamics of the population.

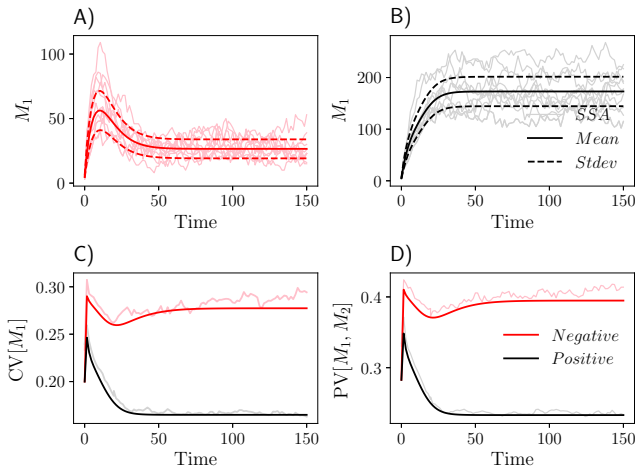


Figure 5: Genetic feedback moment dynamics generated by the symmetry-reduced model (Lognormal MA) for $N = 10$ cells. For negative feedback, $c_i^f = 0.1$ and moments of M_1 are shown in red with 10 SSA realizations (A). For positive feedback, $c_i^f = 1$ and moments of M_1 are shown in black (B). The normalized variance of individual cells and the variance of the difference between two cells are in (C) and (D), respectively. For both feedback cases, the reaction rate parameters and initial conditions are $\langle D_i(0) \rangle = 30$, $\text{Var}[D_i(0)] = 25$, $\langle M_i(0) \rangle = \langle P_i(0) \rangle = \langle DP_i(0) \rangle = 5$, $\text{Var}[M_i(0)] = \text{Var}[P_i(0)] = \text{Var}[DP_i(0)] = 1$, $\langle S(0) \rangle = 5$, $\text{Var}[S(0)] = 0$, $\langle C_i^m \rangle = 0.5$, $\text{Var}[C_i^m] = 0.01$, $\langle C_i^p \rangle = 0.05$, $\text{Var}[C_i^p] = 2.5e-5$, $c^a = 0.01$, $c^d = 0.01$, $d^m = d_p = 0.2$, and $c^{+/-} = 0.8$. Light colored traces in (C-D) are calculated from 2000 SSA realizations.

6 Conclusions

We presented an efficient moment-based approach to study variability in populations of chemically interacting cells. Our approach accounts for both intrinsic and extrinsic sources of variability as well as cell-to-cell coupling via a secrete-and-sense mechanism. In principle, our analysis applies to arbitrary intracellular reaction networks, although its accuracy relies on the availability of suitable closure functions. By exploiting certain symmetries of the resulting moment-equations [13], the number of differential equations needed to describe the population could be strongly reduced. This way, the dimensionality of the model becomes independent of the population size, which enables the analysis of different regulatory processes even in large populations.

References

- [1] D.T. Gillespie ‘A rigorous derivation of the chemical master equation’, *Physica A: Statistical Mechanics and its Applications*, vol. 188, no. 1-3, p. 404-425, doi: 10.1016/0378-4371(92)90283-V, 1992.
- [2] J. Paulsson, ‘Summing up the noise in gene networks’, *Nature*, vol. 427, p. 415-418, 2004.
- [3] A. Hilfinger, J. Paulsson, ‘Separating intrinsic from extrinsic fluctuations in dynamic biological systems’, *Proceedings of the National Academy of Sciences*, vol. 108, no. 29, p. 12167-12172, doi: 10.1073/pnas.1018832108, 2010.
- [4] A. Singh, J.P. Hespanha, ‘Lognormal Moment Closures for Biochemical Reactions’, *Proceedings of the 45th IEEE Conference on Decision and Control*, p. 2063-2068, 2006.
- [5] C. Zechner, J. Ruess, P. Krenn, S. Pelet, M. Peter, J. Lygeros, H. Koepl, ‘Moment-based inference predicts bimodality in transient gene expression’, *PNAS*, vol. 109, no. 21, p. 8340-8345, 2012.
- [6] H. Salis, Y. Kaznessis, ‘Accurate hybrid stochastic simulation of a system of coupled chemical or biochemical reactions’, *The Journal of Chemical Physics*, vol. 122, no. 5, 054103, 2005.
- [7] L. Duso, C. Zechner, ‘Selected-node stochastic simulation algorithm’, *The Journal of Chemical Physics*, vol. 148, no. 16, 164108, doi: 10.1063/1.5021242, 2018.
- [8] A. Ganguly, D. Altintan, H. Koepl, ‘Jump-diffusion approximation of stochastic reaction dynamics: error bounds and algorithms’, *Multiscale Modeling & Simulation*, vol. 13, no. 4, p. 1390-1419, 2015.
- [9] S. Smith, R. Grima, ‘Single-cell variability in multicellular organisms’, *Nature Communications*, vol. 9, no. 1, p. 345, 2018.
- [10] H. Youk, W.A. Lim, ‘Secreting and sensing the same molecule allows cells to achieve versatile social behaviors’, *Science*, vol. 343, no. 1242782, doi: 10.1126/science.1242782, 2014.
- [11] A.M. Stevens, K.M. Dolan, E.P. Greenberg, ‘Synergistic binding of the *Vibrio fischeri* LuxR transcriptional activator domain and RNA polymerase to the *lux* promoter region’, *PNAS*, vol. 91, p. 12619-12623, 1994.
- [12] L.N. Handly, A. Pilko, R. Wollman, ‘Paracrine communication maximizes cellular response fidelity in wound signaling’, *eLIFE*, vol. 4, no. e09652, doi: 10.7554/eLife.09652.001, 2015.
- [13] K. Batmanov, C. Kuttler, F. Lemaire, C. Lhoussaine, C. Versari, ‘Symmetry-based model reduction for approximate stochastic analysis’, in *Computational Methods in Systems Biology*, London: Springer, 2012, p. 49-68.
- [14] Y. Boada, A. Vignoni, J. Picó, ‘Engineered control of genetic variability reveals interplay among quorum sensing, feedback regulation, and biochemical noise’, *ACS Synthetic Biology*, vol. 6, no. 10, p. 1903-1912, 2017.
- [15] D. Schnoerr, G. Sanguinetti, R. Grima, ‘Comparison of different moment-closure approximations for stochastic chemical kinetics’, *The Journal of Chemical Physics*, vol. 143, no. 185101, 2015.
- [16] A. Meurer, C.P. Smith, M. Paprocki, O. Čertík, S.B. Kirpichev, M. Rocklin, A. Kumar, S. Ivanov, J.K. Moore, S. Singh, T. Rathnayake, S. Vig, B.E. Granger, R.P. Muller, F. Bonazzi, H. Gupta, S. Vats, F. Johansson, F. Pedregosa, M.J. Curry, A.R. and Terrel, S. Roučka, A. Saboo, I. Fernando, S. Kulal, R. Cimrman, A. Scopatz ‘SymPy: symbolic computing in Python’, *PeerJ Computer Science*, 3, e103, 2376-5992, 2017.
- [17] K. Choi, J.K. Medley, C. Cannistra, M. Konig, L. Smith, K. Stocking, H.M. Sauro, ‘Tellurium: A Python Based Modeling and Reproducibility Platform for Systems Biology’, *bioRxiv*, 054601, doi: 10.1101/054601, 2016.